



Particle adsorption under irreversible conditions: kinetics and jamming coverage[☆]

Zbigniew Adamczyk *, Paweł Weroński, Elizeusz Musiał

Institute of Catalysis and Surface Chemistry Polish Academy of Sciences, ul. Niezapominajek 8, 30-239 Cracow, Poland

Received 20 June 2001; accepted 15 October 2001

Abstract

Irreversible adsorption of protein and colloid particles at solid/liquid interfaces was analysed theoretically. The expression describing the surface mass balance equation was discussed which can be used as boundary condition for the bulk mass transfer equation. Analytical kinetic equations were derived in the limit of short and long adsorption time. It was shown that the crucial role in the long-time expressions plays the maximum (jamming) coverage which can be derived numerically by applying the random sequential adsorption approach. The results obtained by using this model were discussed in the case of spheres and spheroids. Methods of extending results obtained for hard (noninteracting) particles to interacting particles were also presented. It was demonstrated that the electrostatic double-layer interactions decreased considerably the maximum coverage and influenced the structure of the adsorbed particle mono-layer analysed quantitatively in terms of the pair correlation function. © 2002 Elsevier Science B.V. All rights reserved.

Keywords: Adsorption of colloids; Colloid adsorption; Modelling of particle adsorption; Kinetics of particle adsorption; Protein adsorption

1. Introduction

Effective adsorption of colloids and bioparticles is important for many practical processes such as water and waste water filtration, papermaking, xerography, protein and cell separation, immobilization of enzymes, etc. In other processes, e.g.

membrane filtration, biofouling of membranes and artificial organs, flotation (slime coating formation), production of microelectronic or optical devices, particle adsorption is highly undesirable.

A quantitative analysis of particle adsorption can also furnish interesting information on specific interactions under dynamic conditions which has implications for colloid science, biophysics and medicine, soil chemistry, etc. Furthermore, by measuring particle adsorption in model systems, e.g. mono-disperse colloid suspension, important clues can be gained concerning mechanisms and kinetics of molecular adsorption difficult for direct experimental studies. In this way various

[☆] Special issue devoted to the Polish–Israeli Symposium: ‘Current Trends in Interface Chemistry’.

* Corresponding author. Tel.: +48-12-6395-104; fax: +48-12-425-1923

E-mail address: ncadamcz@cyf-kr.edu.pl (Z. Adamczyk).

aspect of statistical–mechanical theories can be tested and links between irreversible (colloid) and reversible (molecular) systems can be established.

It should be pointed out, however, that despite some analogies protein and colloid particle adsorption is proceeding via more complicated paths than molecular adsorption mostly due to irreversibility effects [1–6]. This means that the adsorption kinetics, maximum mono-layer density (coverage) and its structure depend on particle transport mechanism, either diffusion, convection or migration rather than on particle concentration.

Irreversible adsorption of particles is often analysed in terms of the random sequential adsorption (RSA) model developed in Refs. [7–9] and applied for simulating adsorption of particles of various shape [10–17]. In this work we discuss the applicability of the RSA approach for predicting adsorption of spheroidal particles at solid/liquid interfaces. These theoretical results seem relevant for modelling irreversible protein adsorption whose shape deviates often from a spherical one.

2. Particle adsorption kinetics

It was demonstrated in Refs. [18,19] that the rate of irreversible adsorption of colloid particles can be described in terms of the kinetic equation

$$\frac{d\Theta}{dt} = S_g k_a n(\delta_a) \bar{B}(\Theta) \quad (1)$$

where $\Theta = S_g N$ is the coverage of adsorbed particles, N is the surface concentration of particles, S_g is the geometrical cross-section of the particle, t is the time, $n(\delta_a)$ the particle concentration at the edge of the adsorption layer of thickness δ_a (Fig. 1), k_a is the adsorption constant and $\bar{B}(\Theta)$ is the generalized blocking functions of the adsorbed particle layer. The adsorption constant and the blocking function can be calculated from the following equations when the specific interaction potential particle/interface ϕ is known [19]

$$k_a = 1 \left/ \int_{\delta_m}^{\delta_a} \frac{e^{\phi/kT}}{D(h)} dh \right.$$

$$\bar{B}(\Theta) = 1/k_a \int_{\delta_m}^{\delta_a} \frac{e^{\Phi/kT}}{D(h)} dh = 1/k_a \int_{\delta_m}^{\delta_a} \frac{e^{\phi/kT}}{B(\Theta, h) D(h)} dh \quad (2)$$

where δ_m is the primary minimum distance, δ_a is the thickness of the adsorption layer (Fig. 1), h is the distance between the particle and the interface $D(h)$ the position dependent diffusion coefficient and Φ is the overall interaction potential being the sum of the specific and steric contribution due to adsorbed particles i.e.

$$\Phi = \phi + \phi_s = \phi - kT \ln B(\Theta, h) \quad (3)$$

where $B(\Theta, h)$ is the position dependent blocking function describing the steric interactions between adsorbing and adsorbed particles [19,20].

Eq. (1) describes properly particle adsorption kinetics under the situation when the particle concentration $n(\delta_a)$ remains constant or varies slowly in comparison with the adsorbed layer relaxation time [19]. It can also be used as the kinetic boundary condition for the convective-diffusion equations describing particle transport from the bulk to the adsorption layer [19,20]. However, its application requires the blocking function $\bar{B}(\Theta)$ calculated from Eq. (2). This may be cumbersome because $B(\Theta, h)$ is known for spherical particles in the limit of low coverage only [18].

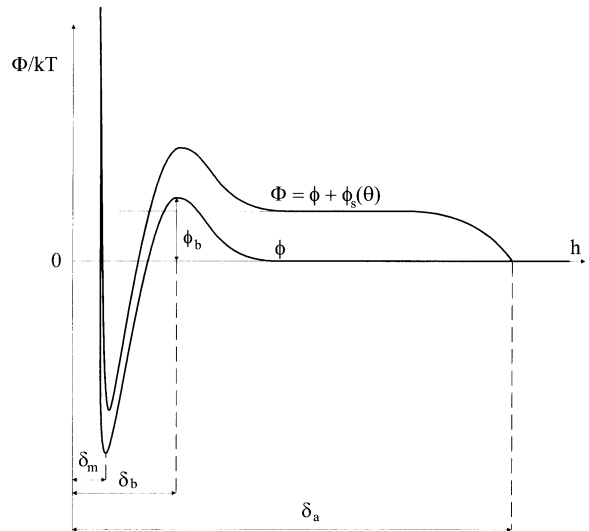


Fig. 1. Schematic representation of the specific ϕ and total Φ energy profiles within the adsorption layer of the thickness δ_a , δ_m is the primary minimum distance and δ_b is the energy barrier distance.

However, as discussed in Refs. [19,20], $\bar{B}(\Theta)$ can well be approximated by the surface blocking function $B_0(\Theta)$ representing the limiting value of $B(\Theta, h)$ when the particle/interface distance tends to zero. For irreversible systems one can determine $B_0(\Theta)$ numerically by applying the RSA model [10–18]. The basic assumption of the model discussed below is that particles are placed (adsorbed) at random with uniform probability over the simulation plane. If the particle finds an empty area it becomes localized permanently. Otherwise, if it overlaps with any previously adsorbed particle, it is not adsorbed. For spherical, noninteracting particles the numerical results can well be approximated by the interpolating function [10]

$$B_0(\Theta) = \left[1 + 0.812 \frac{\Theta}{\Theta_{\text{mx}}} + 0.426 \left(\frac{\Theta}{\Theta_{\text{mx}}} \right)^2 + 0.0716 \left(\frac{\Theta}{\Theta_{\text{mx}}} \right)^3 \right] \left(1 - \frac{\Theta}{\Theta_{\text{mx}}} \right)^3 \quad (4)$$

where Θ_{mx} is the maximum coverage determined a priori from simulations. For noninteracting (hard) spherical particles Θ_{mx} (referred to as the jamming coverage Θ_{∞}) equals 0.547 [17]. For polydisperse suspensions of spherical particles Θ_{∞} was found to increase proportionally to the standard deviation of the size distribution as shown in Ref. [21]. This was also confirmed theoretically for the case of hard discs of low, Gaussian-type polydispersity [22] and for highly polydisperse systems by the power-law distribution [23,24].

On the other hand, for interacting particles, by introducing the concept of the effective interaction range $H^* = h^*/a$ one can approximate Θ_{mx} by the expression [20]

$$\Theta_{\text{mx}} = \Theta_{\infty} f(H^*) \quad (5)$$

where $f(H^*)$ is the function determined numerically as discussed later on.

The low coverage expansion of $B_0(\Theta)$ for spherical particles is [10]

$$B_0(\Theta) = 1 - C_1\Theta + C_2\Theta^2 + 0(\Theta^3) \quad (6)$$

where $C_1 = 4$ and $C_2 = 6\sqrt{3}/\pi$.

It was shown that Eq. (6) is also valid for nonspherical particles with the coefficients C_1/C_2 calculated numerically for various particle shape like spheroids [12,13,15,16] or cylinders and spherocylinders [12,13].

On the other hand, for higher coverages, when $\Theta \rightarrow \Theta_{\text{mx}}$, the blocking function can be approximated by the expression [19,20]

$$B_0(\Theta) \cong C_{\text{mx}}(1 - \Theta/\Theta_{\text{mx}})^m \quad (7)$$

where C_{mx} is the dimensionless constant of the order of unity, $m = 3$ for spherical particles, $m = 4$ for side-on (flat) adsorption of nonspherical particles [12,13] and $m = 5$ for unoriented adsorption of nonspherical particles [15,16].

Knowing $B_0(\Theta) \cong \bar{B}(\Theta)$ one can formulate explicitly the boundary condition and solve the bulk transport equation numerically as done in Ref. [19] for diffusion-controlled adsorption of colloid particles and proteins.

In the case of adsorption from flowing suspensions when the bulk transport becomes stationary after a short transition time, particle adsorption rate can be calculated from the approximate equation derived in Ref. [18].

$$\frac{d\Theta}{dt} = \frac{\bar{B}(\Theta)}{1 + (K-1)\bar{B}(\Theta)} S_g k_a n^b \quad (8)$$

where $K = k_a/k_c$, k_c is the bulk transfer rate constant which has been calculated for various flow configurations [3], n^b is the particle concentration in the bulk.

Using Eq. (8) one can express particle adsorption kinetics in the form of the definite integral

$$(K-1)\Theta + \int_0^{\Theta} \frac{d\Theta'}{\bar{B}(\Theta')} = S_g k_a n^b t = K\tau \quad (9)$$

where $\tau = S_g k_c n^b t$ is the dimensionless adsorption time.

In the special case when $K \sim 1$ which can be realized in practice for micrometer sized particles using the impinging-jet cells [20], Eq. (9) simplifies to

$$\int_0^{\Theta} \frac{d\Theta'}{\bar{B}(\Theta')} = K\tau. \quad (10)$$

Assuming that $\bar{B}(\Theta)$ is in the form of the series expansion given by Eq. (6) one can derive from Eq. (10) the expression

$$\Theta = \Theta_1 \frac{1 - e^{-qC_1\tau}}{1 - \frac{\Theta_1}{\Theta_2} e^{-qC_1\tau}} \quad (11)$$

$$\text{where } \Theta_1 = \frac{C_1}{2C_2}(1 - q), \quad \Theta_2 = \frac{C_1}{2C_2}(1 + q),$$

$$q = \sqrt{1 - \frac{4C_2}{C_1^2}}.$$

On the other hand, for higher coverage, substituting for $\bar{B}(\Theta)$ Eq. (7), one obtains

$$\Theta = \Theta_{\text{mx}} - \frac{\Theta_{\text{mx}}^{m/(m-1)}}{m^{-1}\sqrt{C_{\text{mx}}(m-1)\tau}} \quad (12)$$

For $K \gg 1$ (low transfer rate from the bulk) which is the case for small colloid particles and proteins under forced convection transport conditions, Eq. (9) indicates that the blocking effects governed by the $\bar{B}(\Theta)$ function remain negligible if the inequality is met

$$\Theta < \Theta_{\text{mx}} \left(1 - m \sqrt{\frac{1}{C_{\text{mx}}(K-1)}} \right). \quad (13)$$

In this case particle adsorption kinetics is described by the linear expression

$$\Theta = S_g |j_0| t \quad (14)$$

where $|j_0| = k_n n^b$ is the limiting flux characterising the maximum rate of particle adsorption under a given transport conditions [3].

It should be mentioned that the above results are valid if the hydrodynamic interactions do not affect particle transport through the adsorption layer of the thickness δ_a . This seems justified for smaller colloid particles and proteins. However, for micrometer sized particles placed in shearing flows the hydrodynamic forces play a significant role due to the coupling with the repulsive electrostatic interactions. This leads to enhanced blocking effects called hydrodynamic scattering effects discussed extensively in the recent review works [25,26].

As can be deduced the above kinetic equations can only be applied if the maximum (jamming) coverage Θ_{mx} is known. This parameter can be determined numerically by performing the RSA simulations as discussed below.

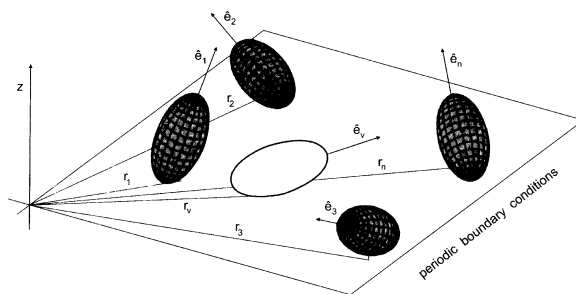


Fig. 2. A schematic representation of the RSA simulations of prolate spheroid adsorption.

3. The RSA simulation method

The RSA simulation algorithm is described in details elsewhere [3,12–16]. The basic features of the model can be characterised as:

- (i) particles of a given shape are placed at random over a square simulation plane of unit area with periodic boundary conditions at its perimeter (Fig. 2); the particle position vector r and the orientation vector \hat{e} are sampled from uniform distributions;
- (ii) if the currently simulated (virtual) particle overlaps with any previously adsorbed particles it is rejected with unit probability and the simulation loop is repeated;
- (iii) otherwise, the particle is assumed irreversibly adsorbed and its co-ordinates and orientation are stored.

Particle adsorption kinetics was simulated by monitoring the number of successful particle adsorption events as a function of the dimensionless time defined as

$$\tau = \frac{t}{t_{\text{ch}}} = \frac{N_{\text{att}}}{N_{\text{ch}}} = \frac{N_{\text{att}}}{(1/S_g)} \quad (15)$$

where N_{att} is the overall number of attempts at placing particles (repetition of the simulation loop) and N_{ch} is the characteristic number of particles.

The maximum coverage Θ_{mx} (referred to as the jamming coverage Θ_{∞} in the case of hard particles) was determined by carrying out the simulation process to the stage when no more particles could be placed at the surface. In order to reduce the excessive computer time needed for attaining

Θ_{∞} , the extrapolation of kinetic runs was used, by exploiting the power-law dependencies of surface coverage on the inverse of adsorption time as predicted by Eq. (12).

The isotropic pair correlation function $g(r)$ was calculated by generating particle populations according to the above RSA scheme and the exploiting the definition

$$g(r) = \frac{S_g \langle \frac{\Delta N_p}{2\pi r \Delta r} \rangle}{\Theta} \quad (16)$$

where ΔN_p is the number of particles found under arbitrary orientation within the ring $2\pi r \Delta r$ drawn around a central particle, r is the radial distance from the centre of this particle and means the ensemble average.

The pair correlation function g can also be expressed in terms of the surface to surface distance h_m which is sometimes advantageous for describing structure of nonspherical particle mono-layer [27]. In this case, $g(h_m)$ was calculated from the equation

$$g(h_m) = \frac{S_g \langle \frac{\Delta N_p}{P_s \Delta h_m} \rangle}{\Theta} \quad (17)$$

where $P_s = 2(P + \pi h_m)$ is the orientation averaged length of the curve formed by rotating a particle (its centre) separated by the distance h_m from the surface of a central particle and P is the particle perimeter [27]. The minimum distance h_m for a given particle orientation was calculated numerically by solving a set of non-linear trigonometric equations.

It should be noted that for spherical particles the centre to centre $g(r)$ and surface to surface $g(h_m)$ correlation functions are the same.

In order to increase the accuracy of g determination, averages from many computer runs were taken in order to attain the total number of particles considered equal 10^5 .

4. Results for numerical simulations

Due to simplicity of the RSA algorithm, numerical simulations for large particle populations can be performed, enabling to determine with a good accuracy both adsorption kinetics, maxi-

mum coverage and structure of adsorbed particle mono-layers.

In this work we focus our attention on spheroidal particle adsorption pertinent to many situations of practical interest. For example, the shape of most surfactant molecules, polymers and globular proteins like bovine serum albumin (BSA) or fibrinogen can be approximated by prolate spheroid with the shorter to longer axis ratio b/a of 0.28 and 0.17, respectively [28–30]. Similarly, various bacteria strains, e.g. the *E. coli* [31] or the bacteria from the *Actinomyces* group resemble prolate spheroids [32]. Adsorption of these particles usually proceeds under irreversible mechanisms which validates the use of the RSA model. It should be noted, however, that the numerical simulations for spheroids are considerable more time consuming in comparison with spherical particles because the particles can adsorb under an arbitrary angle of the longer axis relative to the interface (Fig. 2). The possibility of the unoriented adsorption of spheroidal particles significantly affects the kinetics of this process as can be observed in Fig. 3 which shows the dependence of $\Theta = \tau abN$ on the dimensionless adsorption time τ . The results have been obtained from numerical simulations performed for prolate spheroids with the axis ratio $A = b/a$ equal 0.1, 0.2, 0.5 and 1 (spheres). The value of the constant K was assumed equal one. As can be seen the limiting analytical solutions derived from Eq. (11) describe reasonably well the numerical data for $\tau < 2$. For longer time an apparent saturation of the kinetic curves becomes visible, especially well pronounced for A approaching unity.

Therefore, for longer time, adsorption kinetics can more effectively be presented by using the power-law transformation suggested by Eq. (12). This is clearly visible in Fig. 4 where the dependence of Θ on $\tau^{-1/4}$ is plotted. This transformation has an advantage of compressing the infinite time domain into a finite one. As one can observe, particle coverage becomes indeed a linear function of $\tau^{-1/4}$ with the range of linearity increasing with the A parameter. It should be mentioned, however, that in the case of spheres, the linearity is only observed when using the Θ vs $\tau^{-1/2}$ transformation [9]. The appearance of the

linear adsorption regimes (in the Θ vs $\tau^{-1/4}$ domain) shown in Fig. 4 has a considerable theoretical significance because one can easily determine by extrapolation the jamming coverage Θ_∞ of adsorbed particles. This cannot be achieved directly in calculations due to excessive simulation time.

The dependence of Θ_∞ on the b/a parameter calculated in this way for hard prolate spheroids is presented in Fig. 5. The calculations have been carried out for both the side-on adsorption of spheroids when all particles lie flat at the interface and for the unoriented adsorption (upper curve in Fig. 5).

As can be seen, in the limit of $b/a \rightarrow 1$ (spheres) the jamming coverage in both cases attains the value of 0.547 predicted before [9,17]. It should be noted that this jamming coverage is much smaller than the closest hexagonal packing of spheres in two dimensions which equals $\pi/2\sqrt{3} = 0.91$. On the other hand, for $b/a \ll 1$ the jamming coverage

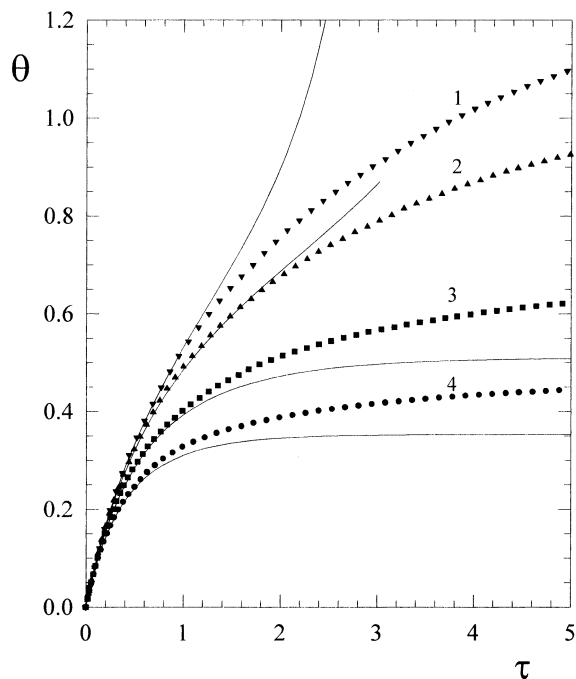


Fig. 3. Adsorption kinetics of hard prolate spheroids; the points denote the RSA simulations performed for (1) $A = 0.1$, (2) $A = 0.2$, (3) $A = 0.5$, (4) $A = 1$ (spheres); the solid lines represent the analytical results calculated from Eq. (11).

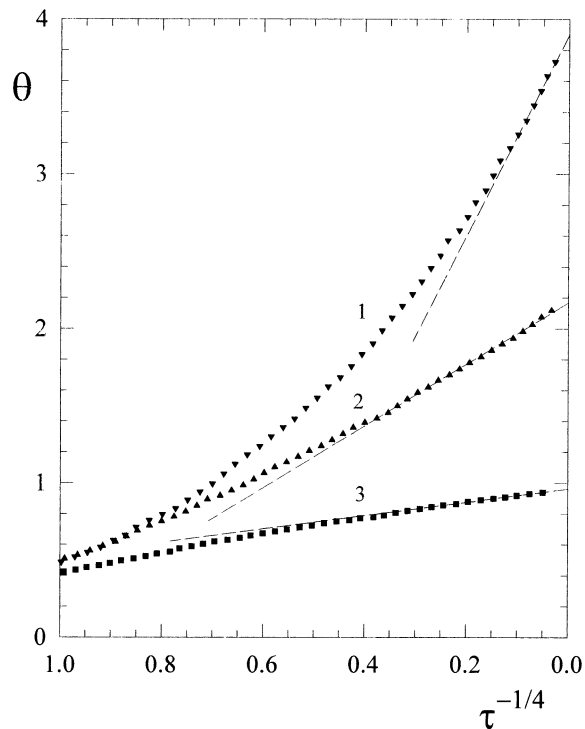


Fig. 4. Adsorption kinetics of hard prolate spheroids expressed in the co-ordinate system Θ vs $\tau^{-1/4}$ the points denote the RSA simulations performed for (1) $A = 0.1$, (2) $A = 0.2$, (3) $A = 0.5$; the dashed lines represent the analytical results calculated from Eq. (12) for $m = 5$.

for unoriented adsorption becomes much larger than for the side-on adsorption which can be attributed to the possibility of a close to perpendicular orientation of the particles which minimizes the area required for their adsorption. In contrast, for the side-on adsorption the jamming coverage decreases with b/a due to geometrical constraints. It was found that the numerical results can well be reflected by the interpolating functions

$$\Theta_\infty = 0.622 \left(A + \frac{1}{A} - 1.997 \right)^{0.0127} e^{-0.0274 \left(A + \frac{1}{A} \right)} \quad (18)$$

for the side-on adsorption and

$$\Theta_\infty = 0.304 - 0.123A + \frac{0.365}{A} \quad (19)$$

for the unoriented adsorption [16].

The data shown in Fig. 5 can be used for determining the influence of particle shape, at fixed volume, on the mass of particle mono-layer. This kind of information is especially important for protein and polymer adsorption when the amount of substance adsorbed is expressed usually in terms of mg per cm². For spherical particles the mass of adsorbed particles per unit area equals

$$m_1 = \frac{4}{3}\rho a\Theta_\infty = 0.729\rho a \quad (20)$$

where ρ is the particle specific density.

For spheroidal particles of the same volume and density one has at the jammed state

$$m_A = \frac{4}{3}\rho b\Theta_\infty(A) \quad (21)$$

Considering Eqs. (18) and (19) the mass ratio m_A/m_1 can be expressed as

$$\frac{m_A}{m_1} = 1.137A^{1/3} \left(A + \frac{1}{A} - 1.997 \right)^{0.0127} e^{-0.0274 \left(A + \frac{1}{A} \right)} \quad (22)$$

for the side-on adsorption of prolate spheroids and

$$\frac{m_A}{m_1} = 0.667A^{-2/3} + 0.556A^{1/3} - 0.225A^{4/3} \quad (23)$$

for unoriented adsorption.

In the case of oblate spheroids (and unoriented adsorption) the expression for the m_A/m_1 ratio becomes

$$\frac{m_A}{m_1} = 0.459A^{-1/3} + 1.404A^{2/3} - 0.865A^{5/3} \quad (24)$$

One can deduce from Eqs. (23) and (24) that in the case of unoriented adsorption of spheroids the mono-layer mass becomes infinite in the limit of $A = b/a$ tending to zero.

The results stemming from Eqs. (22) and (23) are plotted in Fig. 6. Using these data one can determine, in principle, the shape of the adsorbing

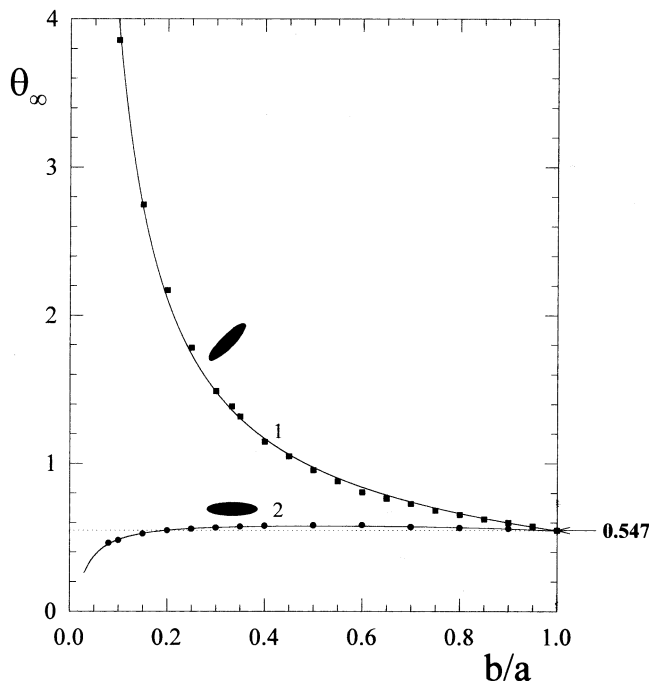


Fig. 5. The dependence of the jamming coverage Θ_∞ of hard prolate spheroids on the parameter $A = b/a$. The points denote the numerical simulations performed according to the RSA model for the unoriented (squares) and side-on (circles) adsorption. The continuous lines show the analytical results derived from the fitting functions given by Eqs. (18) and (19).

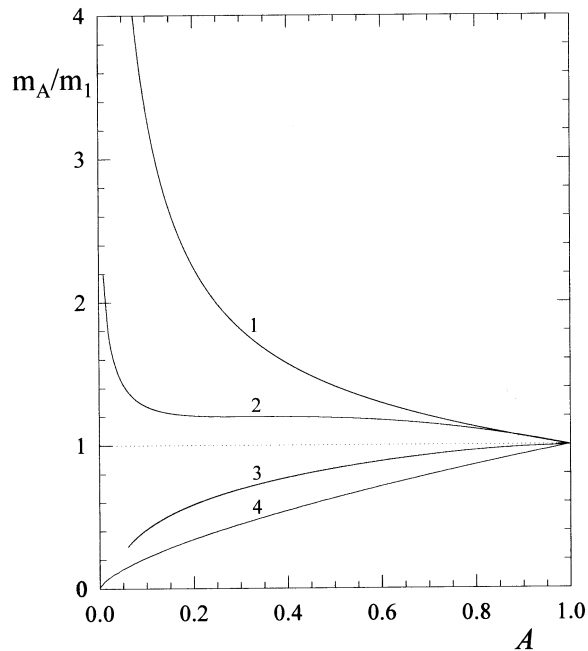


Fig. 6. The dependence of the normalised mono-layer mass m_A/m_1 on the parameter $A = b/a$ calculated from Eqs. (22)–(24) (1) unoriented adsorption of prolate spheroids, (2) unoriented adsorption of oblate spheroids, (3) side-on adsorption of prolate spheroids, and (4) side-on adsorption of oblate spheroids.

molecule, provided that the mass of adsorbed substance is measured experimentally, e.g. by using the radiotracer technique [33].

5. Interacting particle adsorption

All the above results concern the case of hard particle adsorption, when specific interactions among particles were negligible. This adsorption regime is likely to occur for under conditions of concentrated electrolyte solutions when the electrostatic interactions are effectively eliminated, e.g. for protein adsorption under physiological conditions. However, for dilute electrolyte or small particles the repulsive electrostatic interactions may exert a significant influence on particle adsorption, especially on the jamming coverage.

The range of electrostatic interactions is usually characterised by the dimensionless parameter κa defined as

$$\kappa a = (8\pi e^2 a^2 I / \epsilon k T)^{1/2} \quad (25)$$

where e is the elementary charge, I is the ionic strength of the electrolyte solution, ϵ is the dielectric constant of the medium, k is the Boltzmann constant and T is the absolute temperature.

The inverse of the κa parameter has a physical interpretation as the dimensionless Debye screening length $\overline{L_e} = (\kappa a)^{-1}$ [4]. If $(\kappa a)^{-1} < 1$, the range of electrostatic interactions becomes smaller than particle dimension.

The RSA simulations of interacting spheroidal particle adsorption have been discussed elsewhere [16]. It was demonstrated that the complex numerical results can well be interpreted in terms of the effective hard particle (EHP) concept. According to this approach, applied originally by Barker and Henderson [34] to describe the equation of state of simple fluids of spherical molecules, interacting particles are treated as hard ones having larger effective radius $a^* = a + h^*$, where h^* is the effective interaction range.

It was shown [4,16] by performing numerical simulations in the case of electrostatic interactions that for thin double-layers, when the $(\kappa a)^{-1} < 1$, the effective interaction range can be approximated by the linear dependence

$$H^* = h^*/a = \xi (\overline{L_e})^{-1} \quad (26)$$

where ξ is the proportionality coefficient given by [4]

$$\xi = \frac{1}{2} \ln(\phi_0/\phi_{ch}) \quad \text{and} \quad \phi_0 = \epsilon a \left(\frac{kT}{e} \right)^2 Y^2$$

Y is the effective surface potential of the particle and ϕ_{ch} is the characteristic energy close to one kT unit.

For colloid particles, when $\phi_0 = 100$ – 1000 kT, the proportionality constant ξ assumes typical values of 2–3.

Knowing the effective interaction range $H^* = h^*/a$ one can approximate the leading coefficient C_1 of the low coverage expansion, Eq. (6) by the expression [16]

$$C_1(A, H^*) = (2.07 + 0.811A^* + 2.37A^{*2} - 1.25A^{*3})S_g \quad (27)$$

where $A^* = (A + H^*)/(1 + H^*)$,

$$S_g^* = (1 + H^*)(1 + H^*/A).$$

On the other hand, the RSA simulations performed in this work enabled us to formulate the expression for the C_2 coefficient in the form

$$C_2(A, H^*) = p(A^*)C_1^2 \quad (28)$$

where the function $p(A^*)$ is given by the expression

$$p(A^*) = c_1 \left(\frac{A^* - 1}{A^* + c_2} \right)^2 + \frac{3\sqrt{3}}{8\pi}$$

with the coefficients $c_1 = 0.0362$, $c_2 = 0.329$ for unoriented adsorption of prolate spheroids.

In the case of spheres the constants C_1/C_2 assume the simple form

$$C_1 = 4(1 + H^*)^2, \quad C_2 = \frac{6\sqrt{3}}{\pi}(1 + H^*)^4. \quad (29)$$

Knowing the C_1 – C_2 coefficients one can calculate the B_0 blocking function for interacting spheroids and determine particle adsorption kinetics from Eq. (9) or Eq. (11).

It was also demonstrated in Ref. [16] that knowing the constant C_1 for interacting particles one can calculate the maximum coverage Θ_∞^* for prolate spheroids from the expression

$$\Theta_{\text{mx}} = \Theta_\infty \frac{(2.07 + 0.811A + 2.37A^2 - 1.25A^3)}{(2.07 + 0.811A^* + 2.37A^{*2} - 1.25A^{*3})(1 + H^*)(1 + H^*/A)}. \quad (30)$$

For spheres, Eq. (30) reduces to the simple form

$$\Theta_\infty^* = 0.547/(1 + H^*)^2. \quad (31)$$

This simple formula in combination with Eq. (26) defining H^* can be useful for predictions of the ionic strength effect on the maximum coverage of nonspherical particles which is of a primary interest for protein adsorption experiments.

The reduced maximum coverage $\bar{\Theta}_{\text{mx}} = \Theta_{\text{mx}}/\Theta_\infty$ defined by Eq. (30) is compared with exact numerical simulations in Fig. 7 for spheres and prolate spheroids, characterised by $A = 0.5$ and 0.2 , respectively. As can be observed the maximum coverage is considerable reduced for smaller $\kappa a > 5$ values as a result of the lateral interactions

among adsorbed particles. It should be noted that the numerical results are well reflected by Eq. (30) for the entire range of $\kappa a > 5$. The good agreement of simulations with Eq. (30) suggests that for spheres the effective range of interactions H^* can easily be determined experimentally by measuring Θ_{mx} .

Moreover, knowing Θ_{mx} one can calculate using Eq. (12) particle adsorption kinetics in the high coverage limit.

The electrostatic interactions among adsorbed particles influence not only the maximum coverage but also the structure of adsorbed particle mono-layer characterised by pair correlation function g defined above. This can be seen in Fig. 8 showing the mono-layer of hard ($A = 0.2$, $\Theta = 0.98$) and interacting particles ($A = 0.2$, $H^* = 0.1$, $\Theta = 0.98$). Due to electrostatic repulsion more particles are oriented perpendicularly to the interface in comparison with the hard particle

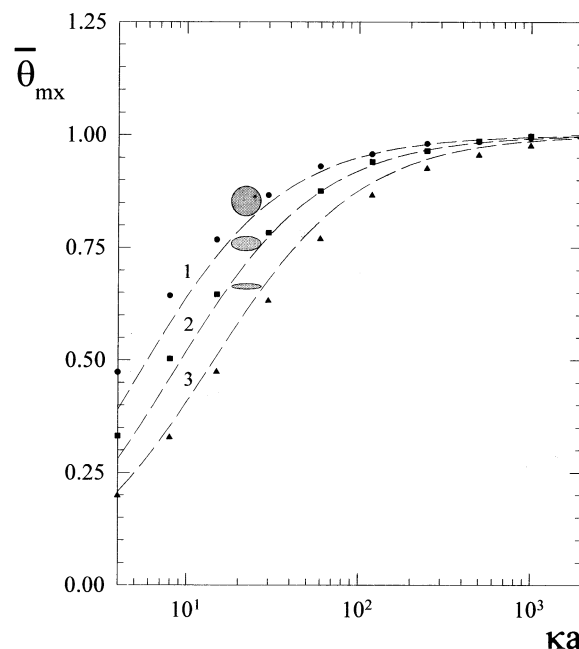
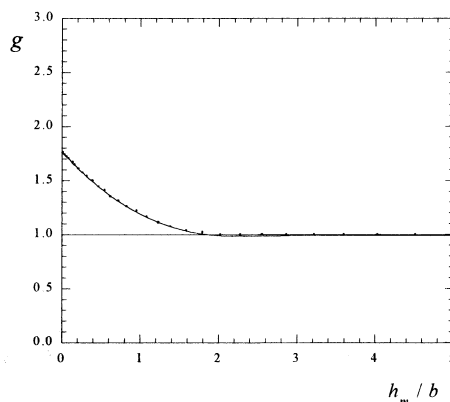
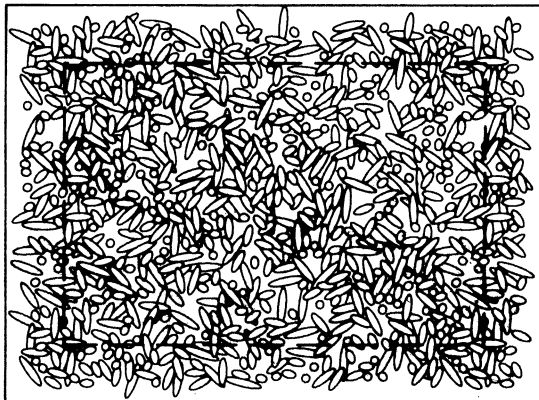


Fig. 7. The reduced maximum coverage $\bar{\Theta}_{\text{mx}} = \Theta_{\text{mx}}/\Theta_\infty$ vs the κa parameter. The points denote the numerical simulations performed according to the RSA model for (1) $A = 1$ (spheres), (2) $A = 0.5$, and (3) $A = 0.2$; the dashed lines denote the analytical approximation calculated from Eq. (30).

a)



b)

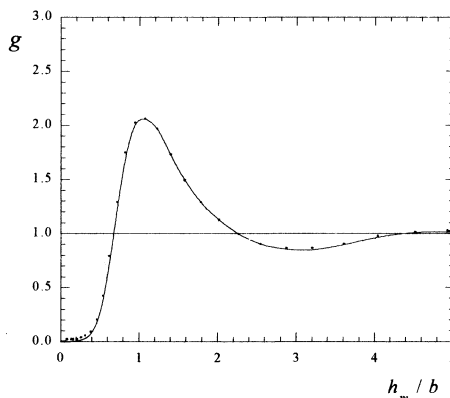
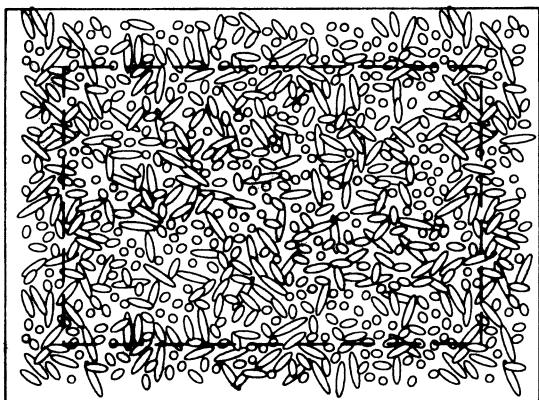


Fig. 8. Part (a) the mono-layer of hard prolate spheroids (RSA simulations performed for $A = 0.2$, $\Theta = 0.98$) and the surface to surface pair correlation function g . Part (b) same as for Part (a) but for the interacting spheroids, characterised by $H^* = 0.1$.

adsorption. Also, the maximum of the pair correlation function is shifted to larger distances in the case of interacting particles. The position of the maximum is closely related to the effective interaction range H^* . Thus, the electrostatic interactions tend to increase the liquid-like short range ordering of particles in the mono-layer. The differences in the structure of the adsorbed particle

mono-layer may have significant practical implications for protein adsorption studies.

As demonstrated in the review works ([3,4,20]) there exist many experimental evidences confirming the validity of the RSA model for describing adsorption kinetics of colloid particles. In particular, the significant influence of the electrostatic interactions on the maximum coverage has been

confirmed by applying the direct microscope observation methods, either optical or AFM [35,36]. Also the structure of the mono-layer was significantly affected by the electrostatic interactions [3,6] in a quantitative agreement with the theoretical predictions stemming from the RSA model. Due to difficulty in synthesising model colloid particles of nonspherical shape all the results discussed in Refs. [3,4,6,20] have been obtained for spherical particles only. However, the usefulness of the RSA model in the case of nonspherical particles seem to be confirmed by the good agreement of the predicted and measured maximum coverage of some globular proteins like BSA, fibrinogen and IgG [19]. Certainly, additional experiments carried out for model colloid systems are needed in order to unequivocally confirm all aspects of the RSA theory in the case of nonspherical particles.

6. Concluding remarks

Irreversible adsorption of large molecules (proteins), clusters and colloid particles can well be reflected in terms of the RSA model. Using this approach one can determine both adsorption kinetics, structure of the mono-layer and the jamming coverage Θ_{∞} , being the parameter of primary practical interest.

The results obtained using the RSA model for hard particles can be used for interpretation of adsorption of interacting particles by introducing the EHP concept. The effective range of interactions h^*/a , being a crucial parameter of this model, is proportional to the double-layer thickness. It has been predicted that the maximum coverage Θ_{mx} is considerably diminished by the lateral electrostatic interactions. Similarly, the mono-layer structure, described by the surface pair correlation function, is significantly affected by the electrostatic interactions.

By exploiting the results presented in this work, especially the maximum coverage for interacting particles, one can determine analytically adsorption kinetics of nonspherical particles using Eqs. (9)–(12) which has implications for protein adsorption studies.

Acknowledgements

This work was partially supported by the EC COPERNICUS Grant: ERBIC 15CT-980121 and the KBN Grant 3T09A10518.

References

- [1] W. Norde, *Adv. Colloid Interf. Sci.* 25 (1986) 267.
- [2] B.R. Young, W.G. Pitt, S.L. Cooper, *J. Colloid Interf. Sci.* 124 (1988) 28.
- [3] Z. Adamczyk, B. Siwek, M. Zembala, P. Belouschek, *Adv. Colloid Interf. Sci.* 48 (1994) 151.
- [4] Z. Adamczyk, P. Warszyński, *Adv. Colloid Interf. Sci.* 63 (1996) 41.
- [5] Z. Adamczyk, B. Siwek, L. Szyk, M. Zembala, *J. Chem. Phys.* 105 (1996) 5552.
- [6] Z. Adamczyk, B. Siwek, M. Zembala, *J. Colloid Interf. Sci.* 198 (1998) 183.
- [7] A. Renyi, *Sel. Trans. Math. Stat. Prob.* 4 (1963) 205.
- [8] J.J. Gonzales, P.C. Hemmer, J.S. Hoye, *Chem. Phys.* 3 (1974) 288.
- [9] E.L. Hinrichsen, J. Feder, T. Jossang, *J. Stat. Phys.* 44 (1986) 793.
- [10] P. Schaaf, J. Talbot, *J. Chem. Phys.* 91 (1989) 4401.
- [11] J. Talbot, G. Tarjus, P. Schaaf, *Phys. Rev. A* 40 (1989) 4808.
- [12] P. Viot, G. Tarjus, S.M. Ricci, J. Talbot, *J. Chem. Phys.* 97 (1992) 5212.
- [13] S.M. Ricci, J. Talbot, G. Tarjus, P. Viot, *J. Chem. Phys.* 97 (1992) 5219.
- [14] J. Talbot, P. Schaaf, G. Tarjus, *Molec. Phys.* 72 (1991) 1397.
- [15] Z. Adamczyk, P. Weroński, *J. Chem. Phys.* 105 (1996) 5562.
- [16] Z. Adamczyk, P. Weroński, *J. Colloid Interf. Sci.* 189 (1997) 348.
- [17] J.W. Evans, *Rev. Modern Phys.* 65 (1993) 1281.
- [18] Z. Adamczyk, B. Senger, J.C. Voegel, P. Schaaf, *J. Chem. Phys.* 110 (1999) 3118.
- [19] Z. Adamczyk, *J. Colloid Interf. Sci.* 229 (2000) 477.
- [20] Z. Adamczyk, P. Weroński, *Adv. Colloid Interf. Sci.* 83 (1999) 137.
- [21] Z. Adamczyk, B. Siwek, M. Zembala, P. Weroński, *J. Colloid Interf. Sci.* 185 (1997) 236.
- [22] J.J. Gray, D.H. Klein, B.A. Korgel, R.T. Bonnecaze, *Langmuir* 17 (2001) 2317.
- [23] N.V. Brilliantov, Y.A. Andrienko, P.L. Krapivsky, J. Kurths, *Phys. Rev. Lett.* 76 (1996) 4058.
- [24] M. Semmler, J. Rička, M. Borkovec, *Colloid Surf. A* 165 (2000) 79.
- [25] Z. Adamczyk, P. Warszyński, L. Szyk-Warszyńska, P. Weroński, *Colloids Surf. A* 165 (2000) 157.
- [26] P. Warszyński, *Adv. Colloid Interf. Sci.* 84 (2000) 47.

- [27] Z. Adamczyk, P. Weroński, *J. Chem. Phys.* 107 (1997) 3691.
- [28] J.Y. Yoon, H.Y. Park, J.H. Kim, W.S. Kim, *J. Colloid Interf. Sci.* 177 (1996) 613.
- [29] B.K. Lok, Yu.-L. Cheng, C.R. Robertson, *J. Colloid Interf. Sci.* 91 (1983) 104.
- [30] P. Schaaf, Ph. Dejardin, A. Schmitt, *Langmuir* 3 (1987) 1131.
- [31] Z. Xia, L. Woo, T.G.M. van de Ven, *Biorheology* 26 (1989) 359.
- [32] R. Bos, H.C. van der Mei, J.M. Meinders, H.J. Busscher, *J. Microbiol. Meth.* 20 (1994) 289.
- [33] J.D. Aptel, J.C. Voegel, A. Schmitt, *Colloids Surf.* 29 (1988) 359.
- [34] J.A. Barker, D. Henderson, *J. Chem. Phys.* 47 (1967) 4714.
- [35] C.A. Johnson, A.M. Lenhoff, *J. Colloid Interf. Sci.* 179 (1996) 587.
- [36] M. Semmler, E.K. Mann, J. Ricka, M. Borkovec, *Langmuir* 14 (1998) 5127.